Thin Solid Films 548 (2013) 425–428

Contents lists available at ScienceDirect

Thin Solid Films

journal homepage: www.elsevier.com/locate/tsf

Surface acoustic wave resonators based on (002)AlN/Pt/diamond/silicon layered structure

Changjian Zhou [a,b,c,*], Yi Yang [a,b], Hao Jin [d], Bin Feng [d], Shurong Dong [d], Jikui Luo [d,e], Tian-Ling Ren [a,b], Mansun Chan [c], Cary Y. Yang [f]

[a] Tsinghua National Laboratory for Information Science and Technology (TNList), Tsinghua University, Beijing 100084, China
[b] Institute of Microelectronics, Tsinghua University, Beijing 100084, China
[c] Department of Electronic and Computer Engineering, Hong Kong University of Science and Technology, Clear Water Bay, Kowloon, Hong Kong
[d] Department of Information Science and Electronic Engineering, Zhejiang University, Hangzhou 310027, China
[e] Centre for Materials Research and Innovation, University of Bolton, Bolton BL3 5AB, UK
[f] Center for Nanostructures, Santa Clara University, CA 95053, USA

ARTICLE INFO

Article history:
Received 6 June 2013
Received in revised form 17 September 2013
Accepted 17 September 2013
Available online 24 September 2013

Keywords:
Aluminum nitride
Diamond
Surface acoustic wave

ABSTRACT

Performance of surface acoustic wave (SAW) resonators based on (002)AlN/Pt/diamond/silicon layered structure is demonstrated. Three resonators with different wavelengths and center frequencies in the GHz range are designed and constructed without using submicron device fabrication processes, due to the high acoustic velocity of the layered structure. The enhanced performance of the SAW resonator by introducing a thin metal layer between the diamond and AlN layers is demonstrated theoretically and experimentally. Dependence of the SAW propagation characteristics on the normalized AlN film thickness is determined and the experimental results are in good agreement with theoretical predictions. In particular, for the 1st wave mode, a very high SAW velocity of 13,656 m/s and an electromechanical coupling coefficient of 0.37% are obtained. These results demonstrate that the (002)AlN/Pt/diamond/silicon layered structure is very promising for high-frequency SAW device applications.

1. Introduction

With the development of high-frequency and high-speed communication systems in the past decade, there is an increasing demand for surface acoustic wave (SAW) devices with higher working frequencies. It is known that the center frequency of a SAW device is determined by $f_0 = V_p / \lambda$, where V_p is the acoustic velocity of the SAW and λ its wavelength. Currently, the SAW devices are fabricated on bulk piezoelectric substrates such as quartz and $LiNbO_3$ which have very low acoustic velocities, and submicron photolithography techniques have to be used to fabricate SAW devices with frequencies in the GHz range. On the other hand, structures composed of a substrate with a high acoustic velocity and a layer of piezoelectric material enable the fabrication of high-frequency SAW devices without the need for such lithography techniques [1–8].

Diamond has a very high acoustic velocity as well as high thermal conductivity, and hence is attractive for high-frequency SAW device application [9–19]. In recent years, various piezoelectric film/diamond/silicon layered structures such as ZnO/diamond/silicon [9], $LiNbO_3$/diamond/silicon [10–12], and AlN/diamond/silicon [13–17] have been studied for SAW applications. The advantages of using diamond are two-fold. First, it hardens the top piezoelectric layer which enhances its acoustic velocity, and second, the acoustic velocity in the diamond layer is high. While ZnO and AlN layers can be readily deposited using sputtering, the preparation of high-quality $LiNbO_3$ film is yet to be developed. Compared with ZnO/diamond/silicon and $LiNbO_3$/diamond/silicon structures, AlN/diamond/silicon is favored for high-frequency SAW devices as it has higher acoustic velocity and smaller velocity dispersion than those in ZnO and $LiNbO_3$ layered structures. In addition, AlN has the advantage of being compatible with integrated circuit (IC) fabrication processes, which makes the AlN/diamond/silicon layered structure very promising as a platform for future semiconductor-on-diamond (SoD) based system-on-a-chip (SoC) that can process high-frequency signals.

In this paper, SAW resonators with different wavelengths are fabricated to study the dependence of SAW properties on the normalized AlN film thickness. The layered structure used in the current study is different from previously reported ones [13–17] in that there is a conducting metal layer between the diamond and AlN films. Theoretical studies on SAW devices using AlN/thin metal film/diamond/silicon structures [18,19] suggested that they perform better than those without a metal underlayer, but no experimental results have been reported to verify such predictions. In this paper, the enhancement of the SAW device performance by using an AlN/Pt/diamond/silicon layered structure is demonstrated theoretically and experimentally.

* Corresponding author. Department of Electronic and Computer Engineering, Hong Kong University of Science and Technology, Clear Water Bay, Kowloon, Hong Kong. Tel.: +852 61597577; fax: +852 23588842
E-mail address: zhoucj86@gmail.com (C. Zhou).

0040-6090/$ – see front matter
http://dx.doi.org/10.1016/j.tsf.2013.09.050

2. Theoretical study

To elucidate the performance enhancement of SAW properties by inserting a metal layer between the diamond and the AlN films, the transfer matrix method is utilized to calculate the SAW propagation characteristics [20,21]. The SAW properties, acoustic velocity V_p and electromechanical coupling coefficient K^2, which depend on the normalized AlN thickness kh_{AlN}, where $k \equiv 2\pi / \lambda$ is the wave number and h_{AlN} is the AlN film thickness, are investigated using this method. Fig. 1(a) shows the axis convention used in the calculation. The diamond layer is modeled as a semi-infinite substrate. If the normalized diamond thickness kh_{dia}, where h_{dia} is the thickness of diamond layer, is larger than 4 [7], it is reasonable to neglect the silicon substrate because the SAW energy is mainly confined in the AlN and diamond films. The layered structure used in our experiment meets this criterion, as illustrated in the ensuing analysis. The material constants used in this calculation have been reported elsewhere [7,22].

To simplify the computations, the SAW is chosen to propagate along the x_1 axis and the upper surface of the diamond layer is at $x_3 = 0$. To describe the SAW properties propagated in the layered structure, a state vector τ is defined as follows.

$$\tau = [T_{13} \quad T_{23} \quad T_{33} \quad D_3 \quad v_1 \quad v_2 \quad v_3 \quad j\omega\phi]^t \tag{1}$$

where T_{i3} (i = 1,2,3) is the ith stress component, D_3 the x_3-component of the electric displacement vector, v_i the velocity component of the vibration, and ϕ the electrostatic potential. All components in the state vector satisfy the continuity condition. Using the piezoelectric constitutive equations and Newton's Law, we can relate the state vector at the upper surface of the AlN film to that at its lower surface using

$$\tau(h_{AlN}) = \exp(j\omega A_{AlN} h_{AlN})\tau(0) = \phi\left(V_p\right)\tau(0) \tag{2}$$

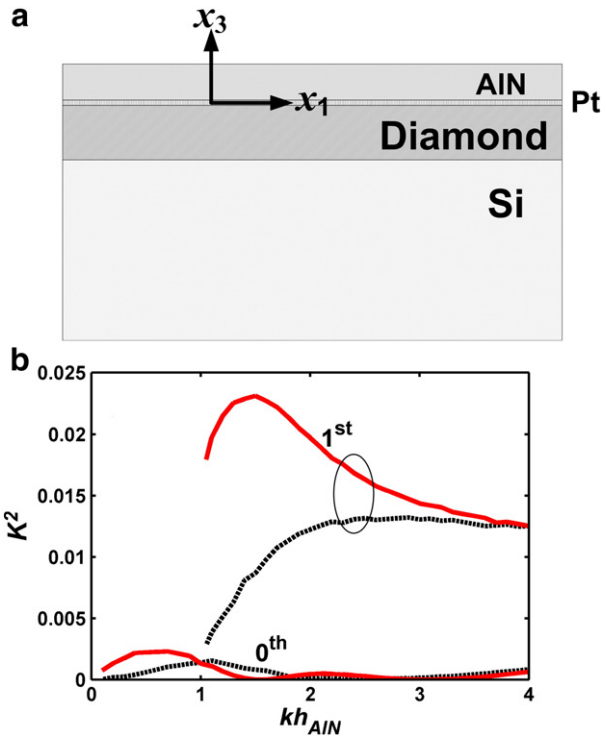

Fig. 1. (a) Cross-sectional schematic of the proposed AlN/Pt/diamond/silicon layered structure and the axis convention used in the computations of SAW properties. (b) Dependence of coupling coefficient K^2 on normalized AlN thickness kh_{AlN} for the layered structures with (red solid lines) and without (black dotted lines) metal interlayer between the diamond and AlN films for the 0th and 1st wave modes.

Table 1
Optimized sputtering conditions.

Parameters	Values
Target substrate distance	70 mm
Base pressure	9×10^{-4} Pa
Working pressure	0.4 Pa
N_2 gas flow rate	65 sccm
Ar gas flow rate	50 sccm
Substrate temperature	450 °C
Sputtering time	60 min
Power	280 W

where the matrix A_{AlN} depends on the SAW acoustic velocity V_p and material constants of AlN, $\tau(0)$ is the state vector at $x_3 = 0$, and Φ the transfer matrix of AlN. $\tau(0)$ can be obtained by applying the boundary condition that the SAW vanishes when $x_3 \to -\infty$ and is given by

$$\tau(0) = \sum_{k=1}^{4} C_k P_k = P\left(V_p\right)C \tag{3}$$

where P_k is the characteristic vector of the matrix A_{dia} for the diamond layer, C_k the weighted coefficient, and $P(V_p)$ and C the matrices composed of the four characteristic vectors and weighted coefficients, respectively.

The coupling coefficients K^2 is given by $K^2 = 2(V_o - V_s) / V_o$, where V_s and V_o are the acoustic velocities obtained with the upper and lower surfaces of AlN short-circuited and open-circuited, respectively. For the short-circuited boundary condition, the state vector $\tau(h_{AlN})$ is given by

$$\tau(h_{AlN}) = [0 \quad 0 \quad 0 \quad D_3 \quad v_1 \quad v_2 \quad v_3 \quad 0]^t. \tag{4}$$

Substituting Eqs. (3) and (4) into Eq. (2), we arrive at

$$[0 \quad 0 \quad 0 \quad D_3 \quad v_1 \quad v_2 \quad v_3 \quad 0]^t = \phi\left(V_p\right)P\left(V_p\right)C. \tag{5}$$

The determinant of the 4 × 4 matrix, a function of V_p and h_{AlN} and composed of rows 1 to 3 and row 8 of the matrix $\Phi(V_p)P(V_p)$ must be zero to ensure that C is a nonzero vector. Given h_{AlN}, we can plot the computed determinant versus V_p, and V_s is the V_p value corresponding to the minimum determinant. Similarly, V_o can be obtained. The insertion of a thin metal layer between the diamond and AlN layers allows us to choose the boundary condition that the electrostatic potential at the interface is zero. Taking this modified boundary condition into account, V_o, V_s, and K^2 for the proposed AlN/Pt/diamond/silicon structure can be computed accordingly. Fig. 1(b) shows the calculated results of

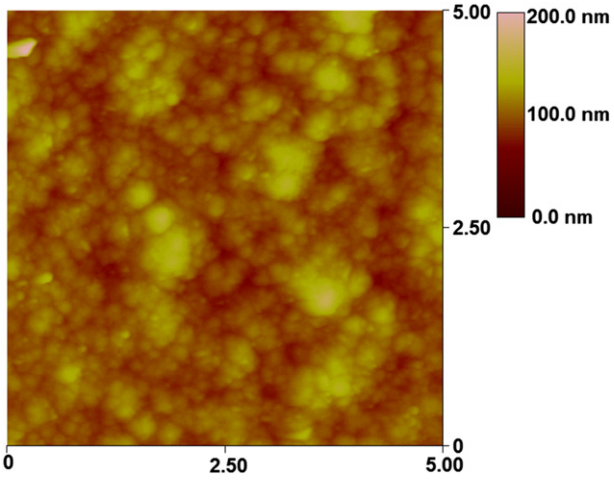

Fig. 2. AFM images of AlN film prepared on Pt/diamond/silicon layered structure.

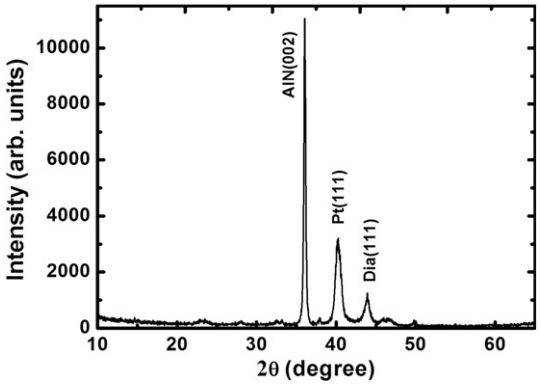

Fig. 3. XRD patterns of AlN/Pt/diamond/silicon layered structure.

K^2 versus the normalized AlN thickness for the layered structures with (solid lines) and without (dotted lines) the metal interlayer between the diamond and AlN films. The enhancement of K^2 by inserting the thin metal layer is apparent, especially for the 1st wave mode.

3. Device fabrication

A polycrystalline diamond film is deposited on a silicon substrate using plasma-enhanced chemical vapor deposition. A 50 nm-layer of platinum is then evaporated onto the diamond-coated silicon wafer, followed by deposition of an AlN layer using DC magnetron reactive sputtering. The thicknesses of the AlN and diamond films are 1.2 μm and 10 μm, respectively. The optimized sputtering conditions to obtain (002)-oriented AlN films are listed in Table 1. Finally, interdigital transducers (IDTs) are formed on the AlN/Pt/diamond/silicon layered structure by depositing a 100 nm-film of aluminum and using conventional photolithography and lift-off processes.

Table 2
Measured characteristics of the three SAW resonators.

	λ(μm)	kh_{AlN}	f_0 (GHz)	V_p (m/s)	$G_m(f_0)$ (10^{-3} S)	$B_s(f_0)$ (10^{-3} S)	K^2 (%)
(a)	12	0.63	1.138	13,656	0.18	23.4	0.12
(b)	7.128	1.06	1.632	11,633	0.16	15.9	0.16
(c)	6	1.26	1.834	11,004	0.40	17.0	0.37

The surface morphology of the AlN film is studied using atomic force microscopy (AFM). Fig. 2 shows the AFM micrograph of the AlN film deposited on the Pt/diamond/silicon layered structure. The root-mean-square roughness of the AlN film is about 11 nm over the measured area of 5 μm by 5 μm, ensuring a sufficiently smooth surface for SAW propagation. Column-like crystalline structure can be clearly observed from the micrograph. Orientations of the AlN and the diamond films are characterized using an X-ray diffractometer (XRD). Fig. 3 shows the XRD patterns of the layered structure. The deposited AlN film exhibits highly preferred (002) orientation, while the platinum and diamond films show only (111) orientations. The rocking curve for the (002) direction of the sputtered AlN film has a full width at half-maximum of 9°, which is slightly larger than that achieved on bare silicon and is comparable to that obtained on Mo, W, and AlSi/Si substrates [23].

Based on the theoretical analysis outlined in Section 2 on the effect of the metal interlayer between diamond and AlN films, we have fabricated three two-port SAW resonators with wavelengths 12 μm, 7.128 μm, and 6 μm, respectively, to study the dependence of SAW properties on the normalized AlN thickness kh_{AlN}. Each resonator has a symmetrical configuration, with its IDT consisting of five pairs of interdigital electrodes, and the distance between adjacent IDTs is 10λ, where the SAW wavelength λ is four times the electrode width. Since h_{dia} is 10 μm, the kh_{dia} values are 5.2, 8.8, and 10.5 for the three SAW resonators, respectively, suggesting that the SAW energy is mainly confined in the AlN and diamond

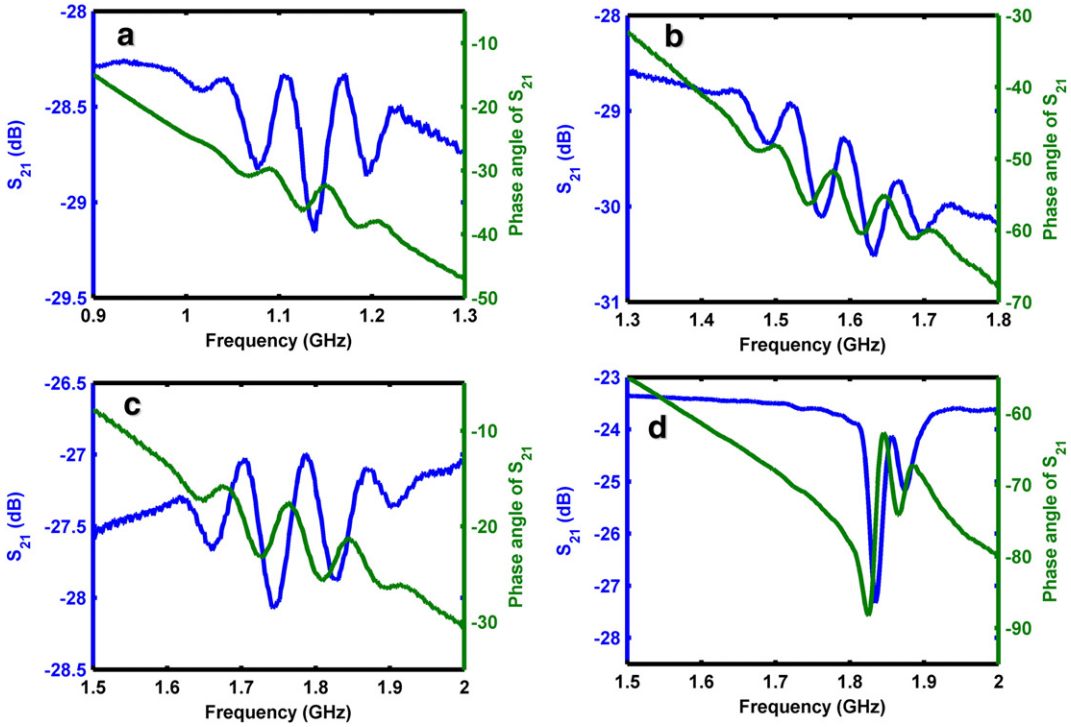

Fig. 4. S_{21} spectra of the fabricated two-port SAW resonators with wavelengths (a) 12 μm, (b) 7.128 μm, and (c) (d) 6 μm. Each transducer consists of 5 pairs of IDTs for devices (a), (b), and (c), while there are 15 and 25 pairs of IDTs in the input and output ports of device (d), respectively.

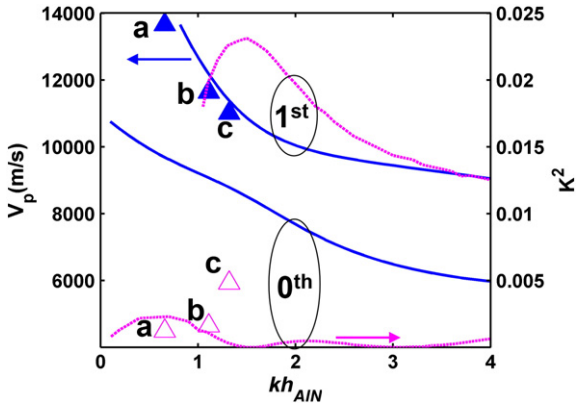

Fig. 5. Comparisons of experimental (data points for the three fabricated resonators a, b, and c) and theoretical (lines) V_p and K^2 for AlN/Pt/diamond/silicon layered structures in 0th and 1st SAW modes. Calculated V_p and K^2 results are indicated by blue solid and pink dotted lines, respectively. Experimental data points for V_p and K^2 in the 1st wave mode are shown with blue solid and pink open triangles, respectively.

layers. Thus the semi-infinite diamond layer assumption in our theoretical analysis is justified under these experimental conditions [7].

4. Results and discussion

Characteristics of the SAW resonators are studied by performing S-parameter measurements using a Rosenberger microwave probe and vector network analyzer over a frequency range of 50 MHz to 2.55 GHz with 1601 sampling data points and an IFBW of 100 Hz. Fig. 4(a), (b), and (c) show the measured S_{21} spectra of the three fabricated SAW resonators. The measured S_{21} spectra take the form of the Sinc function as expected from the uniform IDTs [24]. To suppress the level of the side lobe and obtain a narrower band resonator, one can simply increase the number of the IDT pairs and/or use different IDT pairs for the two ports. Fig. 4(d) illustrates the frequency response of a sample with the same electrode width as sample (c) but having 15 and 25 pairs of IDTs for the input and output ports, respectively. The suppression of the side lobe is significant.

Using the equivalent circuit of a SAW transducer [25], K^2 is given by $K^2 = \pi G_m(f_0) / 4NB_s(f_0)$, where N is the number of finger pairs, and $G_m(f_0)$ and $B_s(f_0)$ are the motional conductance and static susceptance at center frequency f_0, respectively. The SAW properties of the three resonators are summarized in Table 2. The theoretical and experimental V_p and K^2 results for the layered structure are shown in Fig. 5. The theoretical V_p is the average of calculated V_o and V_s as described in Section 2. Note that only the 1st wave mode experimental results are shown for both V_p and K^2 as their experimental values in the 0th mode are very small. All three samples show a V_p larger than 11,000 m/s, with sample (a) exhibiting a remarkably high V_p of 13,656 m/s, clearly demonstrating the hardening effect due to the diamond underlayer. The experimental results for V_p are in excellent agreement with the theoretical predictions. For sample (c), the experimental K^2 value is 0.37%, larger than even the theoretical K^2 value of the SAW device based on conventional AlN/diamond layered structure. However, the K^2 values for all three fabricated resonators in the 1st wave mode are smaller than the theoretical predictions, though they seem to follow the same qualitative trend as the theoretical curve.

The theoretical results are based on the assumption of a single-crystalline c-axis oriented AlN film and obtained using existing data of metalorganic chemical vapor deposited single-crystalline AlN film [22]. However, to conform to current IC fabrication processes, the PECVD diamond film and the sputtered AlN film are both polycrystalline, and thus the AlN film is not perfectly c-axis oriented as used in the calculation. Despite such difference between the theoretical and experimental systems, the measured and calculated acoustic velocities are in excellent agreement. It is clear that the lower experimental coupling coefficients compared with their theoretical counterparts are partly due to an overestimation in the theoretical values resulting from the assumption of a c-axis oriented single crystalline film, which is not expected to be the case in the eventual functional device. Further, in the fabricated device, the propagating acoustic wave is scattered by grain boundaries and surfaces/interfaces within the polycrystalline AlN structure, resulting in attenuation of the SAW energy and measured coupling coefficients lower than the theoretical predictions. Nevertheless, our findings definitively show that the insertion of a metal interlayer does improve the SAW device performance.

5. Conclusion

The SAW propagation characteristics based on the (002)AlN/Pt/diamond/silicon layered structure are investigated theoretically and experimentally. Three SAW resonators with the same geometry but different wavelengths are designed and fabricated on the same substrate to study the dependence of SAW properties on the normalized AlN thickness kh_{AlN}. It is found that the experimental SAW velocities are in excellent agreement with the theoretical predictions. A remarkably high SAW velocity of 13,656 m/s is achieved for $kh_{AlN} = 0.63$, while a SAW velocity of 11,004 m/s with an electromechanical coupling coefficient K^2 of 0.37% is obtained for $kh_{AlN} = 1.26$. The results suggest that the (002)AlN/Pt/diamond/silicon layered structure is very promising as the substrate for future high-frequency SAW device applications.

Acknowledgment

This work was supported by the National Natural Science Foundation (61025021, 60936002, 61011130296) and National Key Project of Science and Technology of China (2009ZX02023-001-3).

References

[1] T.-T. Wu, W.-S. Wang, J. Appl. Phys. 96 (2004) 5249.
[2] K.H. Choi, H.J. Kim, S.J. Chung, J.Y. Kim, T.K. Lee, Y.J. Kim, J. Mater. Res. 18 (2003) 1157.
[3] F. Bénédic, M.B. Assouar, F. Mohasseb, O. Elmazria, P. Alnot, A. Gicquel, Diamond Relat. Mater. 13 (2004) 347.
[4] M.E. Hakiki, O. Elmazria, M.B. Assouar, V. Mortet, L.L. Brizoual, M. Vanecek, P. Alnot, Diamond Relat. Mater. 14 (2005) 1175.
[5] J.G. Rodríguez-Madrid, G.F. Iriarte, D. Araujo, M.P. Villar, O.A. Williams, W. Müller-Sebert, F. Calle, Mater. Lett. 66 (2012) 339.
[6] J.-H. Song, J.-L. Huang, T. Omori, J.C. Sung, S. Wu, H.-H. Lu, D.-F. Lii, Thin Solid Films 520 (2012) 2247.
[7] H. Nakahata, A. Hachigo, K. Higaki, S. Fujii, S. Shikata, N. Fujimori, IEEE Trans. Ultrason. Ferroelectr. Freq. Control 42 (1995) 362.
[8] W.-C. Shih, T.-L. Wang, Y.-K. Pen, Appl. Surf. Sci. 258 (2012) 5424.
[9] H. Nakahana, S. Fujii, K. Higaki, A. Hachigo, H. Kitabayashi, S. Shikata, N. Fujimori, Semicond. Sci. Technol. 18 (2003) S96.
[10] C. Zhou, Y. Yang, J. Zhan, T. Ren, X. Wang, S. Tian, Appl. Phys. Lett. 99 (2011) 022109.
[11] E. Dogheche, D. Remiens, S. Shikata, A. Hachigo, H. Nakahata, Appl. Phys. Lett. 87 (2005) 213503.
[12] T.-C. Lee, J.-T. Lee, M.A. Robert, S. Wang, T.A. Rabson, Appl. Phys. Lett. 82 (2003) 191.
[13] G.F. Iriarte, J. Appl. Phys. 93 (2003) 9604.
[14] J.G. Rodríguez-Madrid, G.F. Iriarte, J. Pedrós, O.A. Williams, D. Brink, F. Calle, IEEE Electron. Device Lett. 33 (2012) 495.
[15] P. Kirsch, M.B. Assouar, O. Elmazria, V. Mortet, P. Alnot, Appl. Phys. Lett. 88 (2006) 223504.
[16] M.B. Assouar, O. Elmazria, P. Kirsch, P. Alnot, V. Mortet, C. Tiusan, J. Appl. Phys. 101 (2007) 114507.
[17] S. Fujii, S. Kawano, T. Umeda, M. Fujioka, M. Yoda, Proceedings of IEEE International Ultrasonics Symposium, 2008, p. 1916.
[18] C.C. Sung, Y.F. Chiang, R. Ro, R. Lee, S. Wu, J. Appl. Phys. 106 (2009) 124905.
[19] C.C. Sung, Y.F. Chiang, R. Ro, R. Lee, S. Wu, Ferroelectrics 48 (2010) 25.
[20] E.L. Adler, IEEE Trans. Ultrason. Ferroelectr. Freq. Control 37 (1990) 485.
[21] E.L. Adler, IEEE Trans. Ultrason. Ferroelectr. Freq. Control 41 (1994) 876.
[22] J.G. Gualtieri, J.A. Kosinski, A. Ballato, IEEE Trans. Ultrason. Ferroelectr. Freq. Control 41 (1994) 53.
[23] S. Mishin, D.R. Marx, B. Sylvia, V. Lughi, K.L. Turner, D.R. Clarke, IEEE Int. Ultrason. Symp. (2003) 2028.
[24] C.K. Campbell, Surface Acoustic Wave Devices for Mobile and Wireless Communications, Academic, San Diego, 1998.
[25] W.R. Smith, H.M. Gerard, J.H. Collins, T.M. Reeder, H.J. Shaw, IEEE Trans. Microw. Theory Tech. MTT-17 (1969) 856.